


# Numerical methods of calculation of stress–strain state of combined elements of sheeting

Dariia Baranetska <sup>1,2,\*</sup>, Maria S. Barabash<sup>3</sup>, Andrii Bieliatynskiy<sup>1</sup>, Olexandr I. Pylypenko<sup>3</sup> and Ihor Mashkov<sup>3</sup>

<sup>1</sup>School of Civil Engineering, North Minzu University, Yinchuan, NingXia, P.R. China

<sup>2</sup>Department of Computer Technologies of Construction, Faculty of Architecture, Civil Engineering and Design, National Aviation University, Kyiv, Ukraine

<sup>3</sup>Department of Computer Technologies of Construction and Reconstruction of Airports, Faculty of Architecture, Civil Engineering and Design, National Aviation University, Kyiv, Ukraine

\*Corresponding author: [dariya\\_baranetska@edu-nau.com.ua](mailto:dariya_baranetska@edu-nau.com.ua)

## ABSTRACT

Steel-reinforced concrete slabs with profiled sheeting are heterogeneous composite structures, therefore, it is necessary to have reliable and practical methods for their calculation, taking into account the heterogeneous structure of structural elements, real load patterns, boundary conditions, etc. The correctness of determining the parameters of the stress–strain state (SSS) of such structural elements depends on considering these factors. In this case, the SSS parameters significantly depend on the transverse displacement deformations influence, and, as a result, deformation of cross sections. Thus, a slab deformation model based on the hypothesis of flat sections may not be suitable for calculating slab with a heterogeneous or composite cross-sectional structure. The calculations conducted according to existing mathematical models indicate stratification of the used materials in practical application and deflection of the slabs in 28% of cases. These calculations ignore the operating features of material stratification and capability loss moments of flanges of profiled sheeting. Therefore, building information modeling (BIM) technologies should be used to calculate such structures and develop practical recommendations for modeling steel-reinforced concrete slabs with profiled sheeting. The finite element method using the LIRA software package allows for clarifying the input of data on the shear moment, the operation of reinforcement, and other materials in a synergistic manner.

**KEYWORDS:** BIM technologies, steel-reinforced concrete, finite element method, deplanation, LIRA-CAD software package

## 1. INTRODUCTION

Bar-reinforced concrete structures are widely used today. The reinforcement in bar-reinforced concrete, as a rule, perceives tensile forces, while the reinforcement operation in the structural member compression zone remains quite effective. Concrete protects reinforcement from corrosion and fire. Reinforced concrete is also known for its high fire resistance. However, there are significant deficiencies in traditional reinforced concrete structures. The main one is the irrational use of concrete in the structural member tensile zone; it does not work here and is ignored when calculating the bearing capacity. The weight of the structure increases significantly due to the forced use of concrete in the tensile zone [1, 2].

The above problem can be partially solved when using prestressed structures [3]. Formwork for cast-in-situ and prefabricated reinforced concrete structures is expensive and irrationally used [4]. Steel structures also have disadvantages [5]. The most important ones are the poor performance of flexible structures or compression members due to the loss of general or local stability, low fire resistance and the need for corrosion protection. These disadvantages can be eliminated or avoided

if rolled stocks and bar-reinforced concrete are connected rationally.

Steel-reinforced concrete structures that combine profiled steel, bar reinforcement and concrete are widely used today due to their high technical and economic efficiency [6, 7]. Steel-reinforced concrete structures best meet the specific requirements for the construction of a particular project and make it relatively easy to solve complex engineering problems. Steel-reinforced concrete is effective in compressed structures, such as pillars or columns, for spanning buildings and structures (slabs, beams, crossbars, trusses, arches, vaults, etc.). It is widely used in the construction of bridges. Sheet reinforcement is a rational choice for steel-reinforced concrete since it performs enclosing and bearing functions simultaneously (tanks, underground, underwater and floating structures) [8].

Various connections of rolled stocks with concrete and reinforced concrete can be used in all these cases, including cast-in-situ and prefabricated slabs on steel profiled sheeting and steel orthotropic deck [9, 10] (Fig. 1).

The properties of steel-reinforced concrete differ from ordinary reinforced concrete, but they can both improve and worsen the structure's performance under load [11–13]. Thus, the

Received: 18 May 2023; Revised: 29 June 2024; Accepted: 20 February 2025

© The Author(s) 2025. Published by Oxford University Press on behalf of Society of Theoretical and Applied Mechanics of the Republic of China, Taiwan. This is an Open Access article distributed under the terms of the Creative Commons Attribution License (<https://creativecommons.org/licenses/by/4.0/>), which permits unrestricted reuse, distribution, and reproduction in any medium, provided the original work is properly cited.

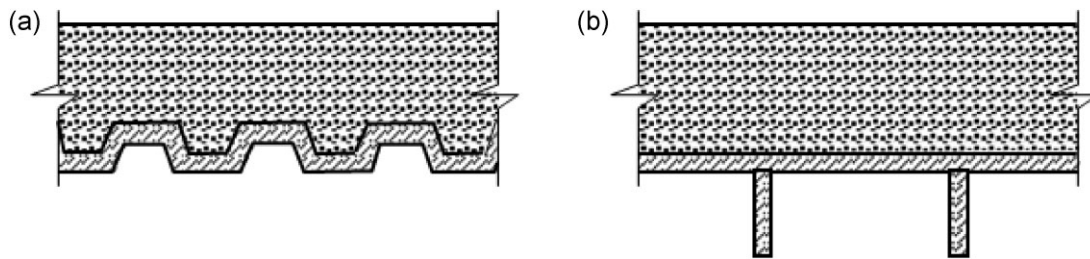


**Figure 1** Cross sections of steel-reinforced concrete slabs: (a) on steel profiled sheeting and (b) on a steel orthotropic deck.

disadvantage is the need to use various anchoring devices to ensure the joint operation of concrete and steel [14]. Nowadays, many structures are reinforced such that a three-dimensional stress state is created in concrete during compression. These structures can be divided into two large groups:

- (1) Structures in which a three-dimensional stress state is created by flexible secondary reinforcement that does not perceive longitudinal forces. These are elements reinforced with conventional and prestressed spirals, collars and cross-sectional meshes. Such solutions are rarely used in steel-reinforced concrete structures.
- (2) Structures reinforced with rigid rebar such that it can absorb longitudinal forces but create a three-dimensional state in concrete, thus increasing its load-bearing capacity ([15, 11]).

The means and mechanisms for ensuring the joint operation of sheet profiled reinforcement with reinforced concrete in combined slabs are still little explored. Since the scope of use of cast-*in-situ* reinforced concrete slabs with sheet reinforcement is expanding, it is necessary to investigate the strength and deformation characteristics of combined slabs on steel profiled sheeting using new anchoring devices.

Decision optimization requires applying an innovative approach to the design, construction and operation of structures and buildings. The solution can be BIM technologies that provide for building a three-dimensional project model and integrating data on structural elements, materials, technological solutions and other aspects of the project. BIM is a methodology for projecting a digital model of a building or infrastructure facility using special software tools. Design in BIM begins with creating a three-dimensional digital model of the project by entering all the necessary parameters and characteristics. Such a model contains information about all project components—from structural elements to operating units. At this stage, designers can visualize and work with the project in three-dimensional space, which, in turn, improves communication between design teams, minimizes errors and speeds up the design process. Creating a 3D model with the LIRA-CAD software package is a reasonable alternative to more expensive foreign programs for strength analysis, such as SAP 2000, STAAD Pro, RISA, RFEM, RSTAB, Robot Structural Analysis, SCIA Engineer, SOFiStiK, etc. Furthermore, it is the best choice for designers, engineers and structural designers among the more affordable MicroFe, LIRA 10 or SCAD Office.

Discussing the technical and economic advantages of using BIM technologies in design is also important. Primary building elements, including load-bearing slabs, are designed in automatic mode when using BIM technologies. BIM technologies also allow designing elements that are erected on the construction site directly, including a foundation, load-bearing walls, roof, and facade structures. The architectural model designed according to technical specifications or sketches and plans is loaded into the program. The program calculates the structural elements of the future facility, creates working drawings, prepares accompanying documents and calculates the final cost sheet. The design of utility services is calculated, and their final layout schemes are entered into the design model, including the illumination standards, heat loss and load-bearing capacity of structures. The program provides a project of the future facility and all works related to its construction. Logistic data is entered into the program, and delivery times for the necessary materials are determined. When the construction is over, the program verifies the constructed facility for its compliance with the BIM model. Moreover, the finished 3D model displays all the adjustments and innovations made during construction. It is easier to make the necessary changes to a digital model than to a paper one. The 3D model designed with the help of BIM technologies makes it possible to synchronize adjustments made at different stages by different experts, track them, and see the result of joint work. The 3D model immediately detects problem areas in the project and eliminates them. Due to this, the probability of errors during construction and the need to eliminate them are reduced to a minimum, which reduces construction costs significantly.

Based on the above, this study aims to improve the calculation methodology using BIM technologies. To do this, it is necessary to solve the following tasks:

- (1) to develop and study ways of joining reinforced concrete with steel profiled sheeting;
- (2) to compare the calculation methods for steel-reinforced concrete slabs with profiled sheeting;
- (3) to determine the strength and deformability of steel-reinforced concrete slabs with profiled sheeting as a fixed formwork;
- (4) to enter the studied designed data into the BIM system using LIRA-CAD software package;
- (5) to develop recommendations for the calculation and design of steel-reinforced concrete slabs with different types of profiled sheeting;
- (6) to compare theoretical and empirical studies of the bearing capacity and deformability of elements.

## 2. RELATED WORK

There are many modern numerical methods to study the stress state, deformations and failure mechanisms of concrete structures under different loading conditions.

### 2.1 Deformation and fracture behavior of concrete under loading

Abdal *et al.* [16] study concrete performance under loading. The researchers establish that longitudinal deformation consists of elastic and plastic ones when stresses reach the tensile ( $R_{bt, ser}$ ) at which the first microcracks are formed, corresponding to the limits of concrete tear resistance. If these stresses exceed the limit, plastic deformations caused by cracks are of primary importance. The tensile strength of concrete overcomes in the transverse direction once it reaches prismatic strength. At the final stage of loading, concrete fractures with the specimen breaking into pieces. In this case, the transverse deformation increment increases at each degree of loading, and the tensile reaches half the value of the longitudinal deformation increment, that is, the coefficient of transverse deformation is equal to 0.5. According to the study, a further increase in the transverse deformation coefficient to 0.8–1.0 is also possible. Thus, the increase in stress from  $R_{bt, ser}$  to  $R_b$  turns microcracks into macrocracks and further leads to concrete destruction with open longitudinal cracks. In triaxial compression, the influence of forces creating a 3D stress state is so strong that it is theoretically impossible to destroy the material. However, the structural integrity of concrete is compromised due to the displacement and sliding of its parts relative to each other. Concrete strength in a 3D stress state is calculated according to the following formula:

$$\frac{\sigma}{R_b} = 1 + \frac{k\sigma_3}{R_{bt}}, \quad (1)$$

where  $k$  is a coefficient that depends on the grade of concrete, ranging from 0.3 to 0.26.

### 2.2 Mathematical modeling of crack development and long-term concrete resistance

A theoretical model suggested by other scientists allows for a differentiated consideration of the long-term resistance of concrete depending on its physical and mechanical properties [17, 18]. The process of long-term destruction is presented as the crack development around round standard pores that are uniformly distributed in a homogeneous mass and are caused by creep. The researchers provide a mathematical description of the crack development process at the macrostructure level [17]. It is noted that inclined cracks of the contact zone initially develop and then change their direction, developing mainly along the compression forces. Cracks start to join gradually under the load increase and form a main crack, which leads to concrete destruction. General longitudinal or transverse deformation under short-term compression consists of deformations that do not affect material soundness and nonlinear deformations caused by crack development. Researchers developed a theoretical approach to calculate the value of concrete longitudinal and transverse deformation. In this case, the formula to calculate the coefficient of transverse

deformations is as follows:

$$\nu_1 \frac{q}{F} + \varepsilon_2 \frac{q}{F + \varepsilon_1} \nu_1, \quad (2)$$

where  $\nu_1$  is a Poisson's ration;  $\varepsilon_1$  and  $\varepsilon_2$  are the relative longitudinal and transverse deformations caused by concrete fracture and  $q$  is a reduced load.

Hong *et al.* [19] establish that cracks expand even with constant external stresses under prolonged load exposure due to concrete creep. The researchers developed formulas to determine the time until concrete fracture (long-term strength). Such researchers as Sánchez-Olivares and Tomás [20], Yu *et al.* [21] and Wang *et al.* [22] developed a mathematical description of crack development under biaxial and triaxial compression and short-term and long-term load action. According to these studies, in the case of triaxial compression ( $\sigma_1 > \sigma_2 = \sigma_3$ ), the lateral pressure coefficient ( $k$ ) varies widely depending on the magnitude of the lateral pressure. The values of  $k$  significantly exceed the usually accepted value of 4 at low lateral pressure, when destruction occurs mainly by tearing. The values of  $k$  decrease, approaching 4 at higher lateral pressure, when destruction is predominantly of a landslide nature.

According to Wang *et al.* [23], the lower strength of cellular aggregate concrete under triaxial compression is due to the following factors: the “limiting” role of the weak aggregate (when it shows its greatest strength in concrete), the significant homogeneity of concrete and the multifactorial effect of the concrete structure and its smaller plastic deformations. In the case of elastic deformations, all external force energy on the element deformation is converted into its potential energy. The element, when it is released from the external load, restores to its original state. Plastic deformations are caused by the fracture of part of the internal connections and the formation of new ones. At the same time, the external force energy is irretrievably spent on these transformations in the structure.

The irregular arrangement of particles that make up concrete in the placement and size of pores leads to a dispersion of its strength. Thus, modern numerical methods for heterogeneous structures should also consider technological factors, the age and conditions of curing, the shape and size of the specimen, load duration and the type of stress state.

### 2.3 Numerical methods for analyzing concrete structures

The finite element method (FEM) was selected to calculate steel-reinforced concrete slabs with profiled sheeting due to its ability to discretize complex geometries into smaller elements, enabling precise modeling of material heterogeneity, nonlinearities and localized phenomena like crack growth and creep under varied loading conditions.

The theoretical basis of the LIRA software package was the FEM, implemented in the form of displacements [24]. This form was selected due to the simplicity of its algorithmization and physical interpretation, the unified methods for constructing stiffness matrices and overload vectors for different types of end parts, the ability to consider random boundary conditions and the complex geometry of the calculated structure.

The FEM is more complex to implement than the finite difference method. The FEM, however, has many advantages that are

demonstrated when solving real problems. For example, when it comes to the arbitrary shape of the processed area or the possibility of making the finite element mesh sparser in places where special accuracy is not needed. This advantage made a comparison with the finite difference method unnecessary. The use FEM was unpopular for a long time due to the lack of algorithms for automatic partitioning into “almost equilateral” triangles (the error, depending on the method, is inversely proportional to the sine of either the most acute or the most obtuse angle in partitioning). This problem was successfully solved by the algorithms based on the Delaunay triangulation, which made it possible to create fully automatic finite element CAD systems. The domain where differential equations are solved is divided into a finite number of elements. The type of approximating function is arbitrarily selected in each of the elements. In the simplest case, this is a first-degree polynomial.

Outside its element, the approximating function is equal to zero. The values of functions on the boundaries of elements (at nodes) represent the solution to the problem but are unknown in advance. The coefficients of approximating functions are usually found from the condition of equality of the values of neighborhood functions on the boundaries between elements (at nodes). These coefficients are then expressed through the values of the functions at the nodes of the elements. A system of linear algebraic equations is compiled. The number of equations is equal to the number of unknown values at the nodes at which the solution of the original system is found; it is directly proportional to the number of elements and is limited only by electronic computer capabilities. Since each element is connected with a limited number of neighborhood elements, the system of linear algebraic equations has a sparse form, which significantly simplifies its solution. Given the present stage of development allows computing technology to enter large arrays of data, the limitations of the computer's system capabilities are conditional.

The implemented version of the FEM used the principle of possible displacements

$$a(u, v) = (f, v), \quad (3)$$

where  $u$  is the desired exact solution;  $v$  is any possible displacement and  $a(u, v)$  and  $(f, v)$  are possible work of internal and external forces, respectively.

The area occupied by the structure was divided into finite elements ( $\Omega_r$ ), and nodes and their degrees of freedom ( $L_i$ ) (displacement and angles of node rotation) were assigned. The degrees of freedom corresponded to the basis (coordinate, approximating) functions ( $\mu_i$ ), which satisfied the equation

$$L_j \mu_i = \begin{cases} 1, & i = j \\ 0, & i \neq j \end{cases}. \quad (4)$$

An approximate solution was sought as a linear combination of basic functions

$$U_h = \sum_{i=1}^N u_i \mu_i, \quad (5)$$

where  $U_i$  stands for numbers;  $N$  is the number of degrees of freedom.

The FEM was further used to solve the linear problem since the nonlinear problems were resolved into a sequence of linear ones. After  $U$  was substituted with  $U_k$  and  $v$  was substituted with  $\mu_j$  ( $j = 1 \dots N$ ), a system of FEM equations was obtained

$$\sum_{i=1}^n u_i a(\mu_i \mu_j) = (f, \mu_j), \quad i = 1, \dots, N. \quad (6)$$

The stiffness matrix was signified as  $K$  with the following elements:  $k_{ij} = \alpha(\mu_i, \mu_j)$ ;  $P_i = (f, \mu_i)$ , which is a load vector;  $X$ , which is a search vector with elements  $u_i$ . This equation was written into the system in the matrix form ( $KX = P$ ). Thus, the FEM helped to solve the problem within a system of linear algebraic equations.

Once this problem was solved, the vector  $X$  and other stress-strain state (SSS) compensators were calculated. The advantage of the above method is that the  $K$  matrix and the  $P$  vector were obtained by summing the corresponding elements of stiffness matrices and load vectors constructed for individual finite elements. Such a theoretical justification allowed the verification of the correctness of known finite elements. Furthermore, it was possible to develop principles for constructing new compatible and incompatible elements and to obtain error estimates for them.

When solving the problem of bending thin plates, FEM relied on the Kirchhoff-Love hypothesis ( $e_{xz} = e_{yz} = 0$ ), the vertical displacement theory, and the hypothesis of zero transverse pressure ( $\sigma_z = 0$ ). The function of the total potential energy of a bent plate was calculated according to the following formula:

$$P(w) = \frac{1}{2} \iint_{\Omega} (M_x X_x + M_y X_y + 2M_{xy} X_{xy}) d\Omega - \iint_{\Omega} f w d\Omega, \quad (7)$$

$$M_x = \int_z \sigma_z z dz, \quad (8)$$

$$M_y = \int_z \sigma_y z dz, \quad (9)$$

$$M_{xy} = \int_z \tau_{xy} z dz. \quad (10)$$

Linear bending moments about the  $Y$  and  $X$  axes and linear torque moment were calculated according to the following formula  $X$  and  $Y$

$$X_x = \frac{d^2 w}{dx^2}, \quad (11)$$

$$X_y = \frac{d^2 w}{d\delta y^2}, \quad (12)$$

$$X_{xy} = \frac{d^2 w}{dx dy}, \quad (13)$$

where  $f(x, y)$  is a function of internal load, orthogonal to the middle surface of the plate;  $w(x, y)$  is a function of deflections over the middle surface of the plate;  $Z$  stands for a section  $[-\frac{\delta}{2}, \frac{\delta}{2}]$

Relative linear and angular deformations ( $e_x, e_y, e_{xy}$ ) over the curve were calculated as follows:

$$e_x = \frac{du}{dx} = -\frac{d^2w}{dx^2}z = -zX_x, \quad (14)$$

$$e_y = \frac{dv}{dy} = -\frac{d^2v}{dy^2}z = -zX_y, \quad (15)$$

$$e_{xy} = \frac{du}{dy} + \frac{dv}{dx}z = -2z\frac{d^2w}{dxdy} = -2zX_{xy}. \quad (16)$$

For a plane stress state, deformations and stresses are related to each other. For the case of plane deformation,  $E$  and  $\nu$  are replaced by  $\frac{E}{(1-\nu^2)}$  and  $\frac{\nu}{(1-\nu)}$ , respectively, and  $\sigma_z = \nu(\sigma_x + \sigma_y)$  is calculated.

The Pasternak elastic foundation (two-parameter) model was used to calculate slabs and shells lying on an elastic foundation, where  $C_1$  and  $C_2$  constants characterized the operation of the elastic foundation in compression and shear. The Winkler elastic foundation (one-parameter) model could be obtained provided that  $C_2 = 0$ . The system potential energy was calculated according to the following formula:

$$U = P + P_1 \quad (17)$$

where  $P$  is the potential energy of the structure that depends on the type of structure;  $P_1$  is the potential energy of the elastic foundation that contacts with the structure. They were determined according to the following formula:

$$P_1 = \frac{1}{2} \iint_{\Omega} \left\{ C_1 w^2 + C_{2,x} \left( \frac{dw}{dx} \right)^2 + 2C_{2,xy} \left( \frac{dw}{dx} \cdot \frac{dw}{dy} \right) + C_{2,y} \left( \frac{dw}{dy} \right)^2 \right\} d\Omega. \quad (18)$$

The Finite Element Library (FEL) contains elements that simulate the operation of various types of structures: rod elements, quadrangular and triangular elements of a plane problem, plates, shells, elements of a spatial problem—tetrahedron, parallelepiped and trihedral prism. After the given construction is presented in the form of a finite element scheme, the problem of determining the displacements of nodes is reduced to solving a system of algebraic linear equations

$$\mathcal{K}q = F, \quad (19)$$

$$AX = B, \quad (20)$$

$$N * N X k * N = N * k, \quad (21)$$

where  $A$  is a symmetric positive definite matrix of  $N * N$  size;  $B$  is a right-hand-side matrix of  $N * k$  size, where  $k$  is number of sides;  $X$  is a desired displacement matrix of  $k * N$  size.

Since the  $A$  matrix is sparse in most cases, the variables are primarily ordered to minimize the matrix profile and reduce the required RAM, external memory and computation time. All finite elements included in the FEL are theoretically substantiated; their error estimates in stress and displacement are obtained. The stress error estimate is proportional to  $h\tau$ , where  $h$  is the maximum size of finite elements,  $\tau$  is equal to 2 for rect-

angular plate elements and  $\tau$  is equal to 1 for other elements. The displacement error estimate is proportional to  $ht$ , where  $t$  is equal to 4 for rectangular plate elements, and  $t$  is equal to 2 for other elements. When solving a flat stress problem, the FEM relies on generally accepted hypotheses about the absence of deformations or stresses ( $\varepsilon_z, \gamma_{xz}, \gamma_{yz} = 0$ ).

## 2.4 Recommendations for modeling steel-reinforced concrete slabs using FEM

Considering the various software packages that calculate the SSS by the FEM, the most common and powerful is LIRA-CAD. The capabilities of this program are perfect for scientific research, including building a model of finite elements, nonlinearity, contact of materials, etc. In this subsection, attention is paid to the calculation and study of the SSS of steel-reinforced concrete slabs by the FEM. The SSS will be studied by the FEM experimentally for all types of slabs and at each of their points. The study will define the procedure for preparing 3D geometry for meshing and the procedure for applying material models, types of finished elements, loads and boundary conditions, material contact and others.

A prerequisite for modeling is a contact layer between concrete and profiled sheeting that simulates delamination and allows studying its effect on the slabs' SSS. According to specimen experiment conditions, the SSS should be determined at each point of the profiled sheeting or slab. A 3D FEM model should be used, considering the shape of the section. Accordingly, 3D modeling requires designing 3D geometric models of both profiled sheeting and heavy concrete. Meshes of solid finite elements in the shape of hexahedra and prisms are used to simplify calculations and increase their accuracy. This approach helps reduce the number of errors when meshing and in the geometry of the elements themselves.

Since profiled sheeting is a geometric object consisting of thin plains, flat (2D) finite elements were used to model it. The choice of flat finite elements was substantiated by insignificant changes in the parameters of thickness stress of profiled sheeting, which were not the subject of this research. It was decided to single out the following components from the analysis of slab design: profiled sheeting, mass concrete, reinforcement and contact. An appropriate type of finite element was used to simulate each constituent. 1D finite elements were used to model reinforcement, 2D finite elements were used for profiled sheeting and 3D finite elements—mass concrete and contact. As a result, models with 1D, 2D and 3D finite elements interconnected at nodes were designed. The combination of different types of finite elements in one model helps simplify it but preserves the accuracy of calculations, facilitates data processing and reduces the calculation time.

When studying the SSS of P-1, P-2 and P-3 slabs, an attempt was made to use 3D finite elements for modeling profiled sheeting; the authors strived to determine the influence of the type of finite element on the accuracy of calculations. The contact layer was modeled using 3D finite elements and combined 3D finite elements of heavy concrete and 2D finite elements of profiled sheeting. Original drawings of profiled sheeting and steel-reinforced concrete slabs were used to design finite element models.

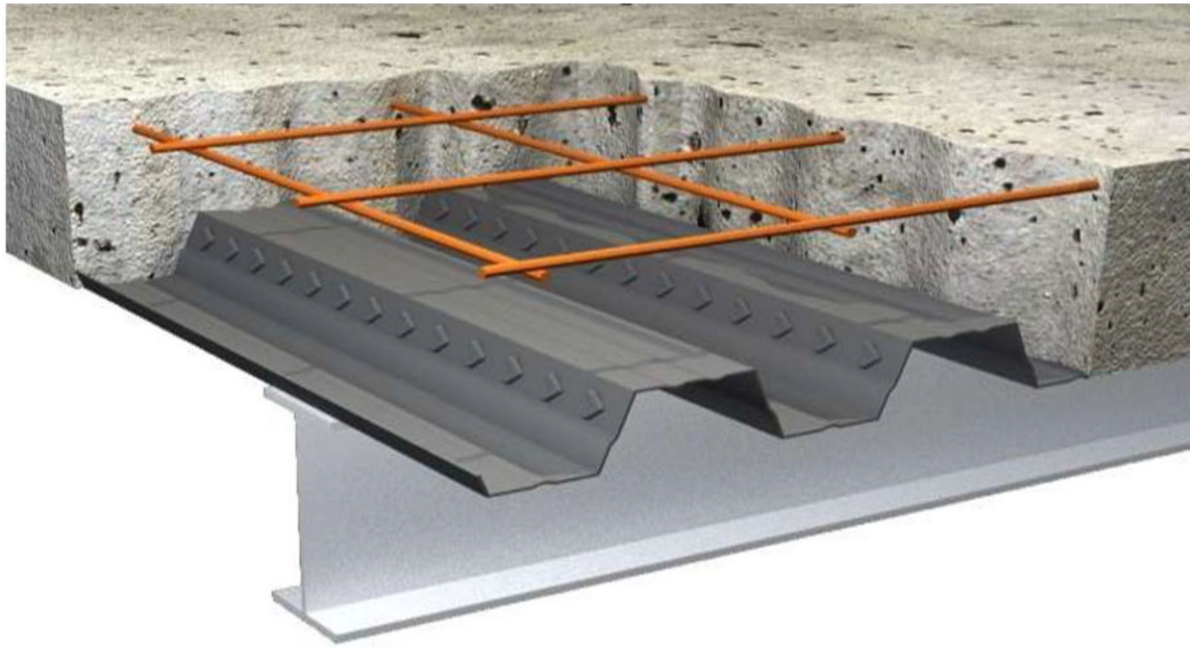


Figure 2 Steel-concrete slabs.

### 3. METHOD

The paper considers cast-*in-situ* slabs with profiled sheeting. Reinforcement was loaded in a concrete slab the same as with standard formwork. This method significantly reduced construction costs compared to prefabricated slabs and sped up the process compared to standard cast-in-site structures. When tensile forces are perceived, the profiled sheet starts to participate in their distribution. This is achieved through special fastening methods, such as the use of special notches or holes on the corrugated walls (Fig. 2).

In order to calculate case-*in-situ* slabs for profiled sheeting, it is necessary to separate the construction and operation stages and consider their interplay. Steel profiled sheeting acts as formwork at the construction phase, bearing the load from its weight, concrete and other erection works. It is calculated in accordance with the standards. There is no need to consider the height of protrusions and dents in sheeting for the working area of steel profiled sheeting unless tests confirm that the working area is large. The bearing bending capacity of the cross sections of steel-reinforced concrete slabs along profiled sheeting should be determined using a simplified method. However, the common bending analysis can be used as an alternative method of calculation.

The authors of this article designed specimens of case-*in-situ* slabs on profiled sheeting. They were rectangular (800 × 1200 mm), formed by supporting profiled sheeting (H85-850-0.8) with zinc coating. A 40 mm thick case-*in-situ* concrete slab filled with corrugations was installed on the top of the coating. The authors used profiled sheets with stampings of different profiles in P2 and P3 specimens. Reinforcing cages were used in P3 specimens. P2 and P3 specimens also differed in storage conditions. P2 specimens were tested after being in laboratory conditions, while P3 specimens were exposed to atmospheric influences for 365 days.

Along with the corresponding specimens, three sets of standard concrete cubes (100 × 100 × 100 mm) and prisms (100 × 100 × 400 mm) were produced to determine the physical and mechanical properties of the concrete composition. All produced specimens were stored in laboratory conditions, where the temperature was 15–18°C, and relative humidity reached 70–75% until they reached the designed strength of concrete. P3 slabs were then moved to the open air. Specimens were tested upon reaching the design strength of concrete at the curing age of 28 days. Tests were carried out under short-term loading on presses and laboratory test benches.

The concrete and metal surfaces of specimens were scraped with rubbing brick and sandpaper of different fineness before electric resistance strain gauges were glued on them. The surface was degreased with acetone and an alcohol solution. After drying, the surface was primed with several coats of BF-2 glue. The underside of the electric resistance strain gauge and capacitor paper were coated with glue, which prevented the sensor from short-circuiting with the metal surface. The electric resistance strain gauge was applied to the spread glue coat after 1 or 2 min according to the markup through a 0.02 mm thick cellulose film gasket (Fig. 3).

The physical and mechanical strength characteristics and deformability of sheet steel were determined on sheet strips cut off from the remnants of sheets of a given batch and processed in accordance with the requirements.

### 4. RESULT

The similarity between BIM and 3D modeling is that the design of a building is created in three-dimensional space. In contrast to 3D modeling, BIM is directly linked to the database. BIM model includes not only load-bearing lines and texture of materials but also technological data of the building. BIM considers the



Figure 3 Placement of electric resistance strain gauges.

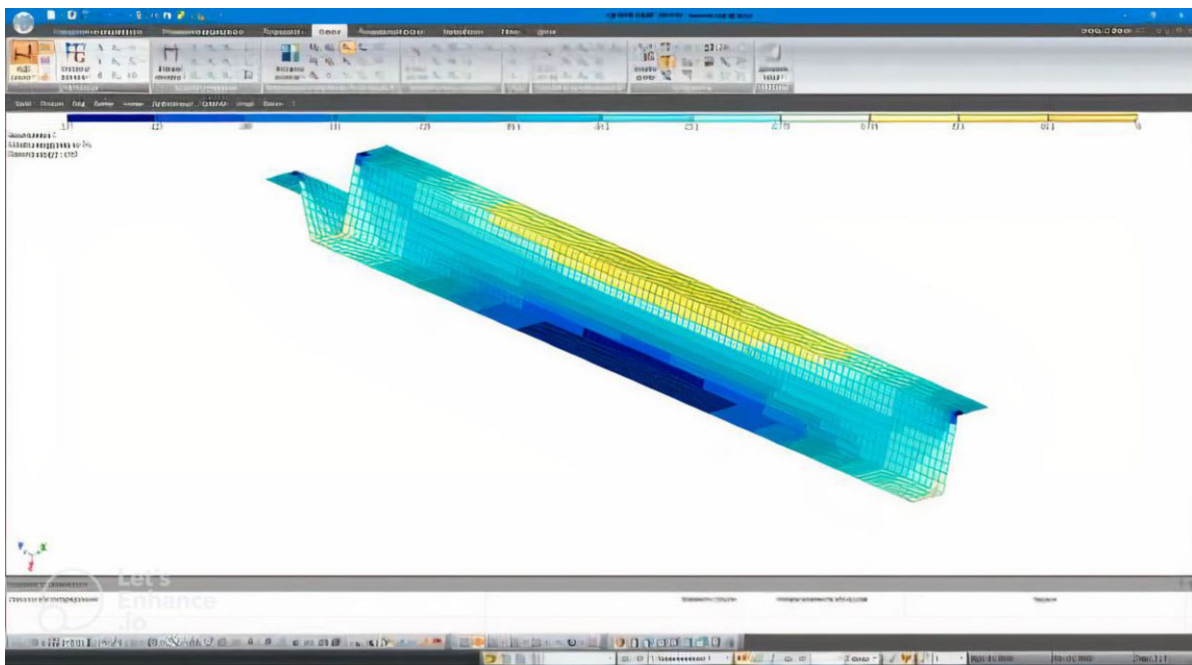


Figure 4 3D geometric model of H-85 profiled sheeting.

physical characteristics of an object and its placement in space. Using the LIRA-CAD software package as a BIM technology provides for the graphic systems analysis, export of objects from Revit, and import into industry foundation class, including recognition of structural sections.

#### 4.1 Geometric model of steel profiled sheeting

As mentioned above, 2D finite elements were used to model profiled sheeting. Such finite elements were overlapped with planes or shells. The geometric model was designed in the LIRA-CAD software package by constructing a profile line and “stretching” it into interconnected planes and surfaces (Fig. 4). The length of the profiled sheeting was equal to 1500 mm, corresponding

to the length of the specimens. A similar approach was used for modeling profiled sheeting when studying slabs.

A geometric model of profiled sheeting was designed in the shape of a 3D body for P-1, P-2 and P-3 slabs. The model was built as a 0.7 mm thick plane, corresponding to the profile of profiled sheeting. This model was then “stretched” to a length of 1500 mm using the LIRA-CAD software package.

#### 4.2 Geometric models of P-1, P-2 and P-3 slabs

One-dimensional, two-dimensional and three-dimensional finite elements were used to calculate the slabs. Geometric models for composite slabs were designed in accordance with the type of finite element. Three-dimensional bodies were used for mass concrete and contact, the extreme lower planes of the built

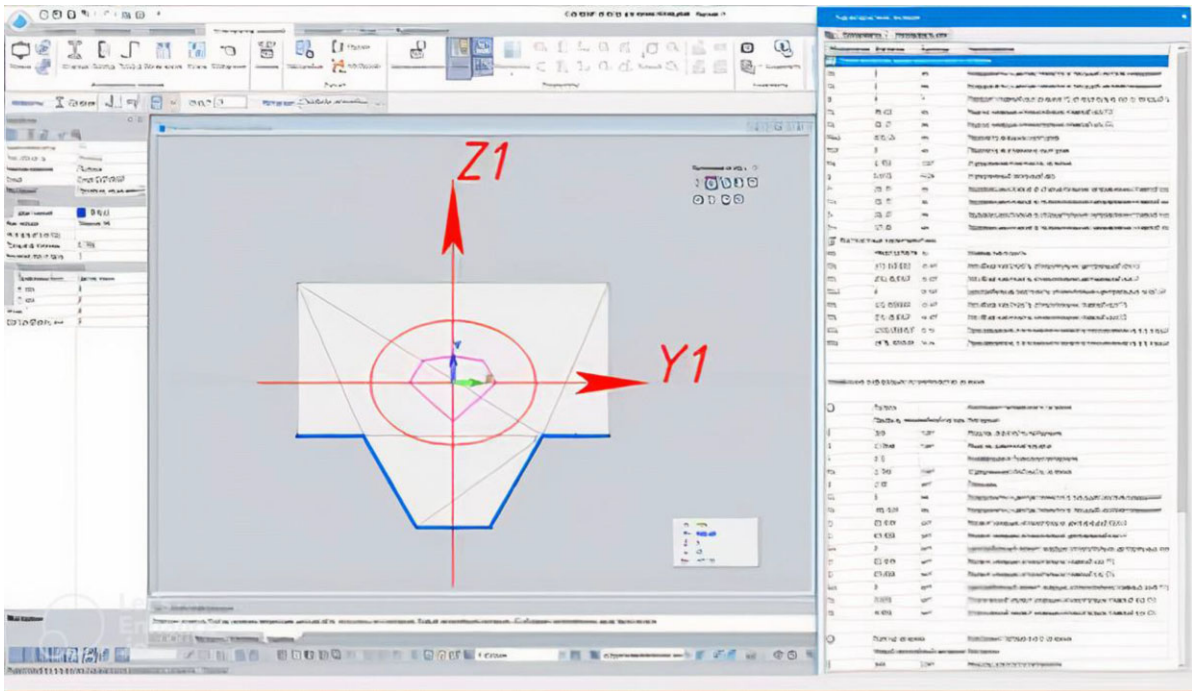


Figure 5 Geometrical characteristics of the section of the P-1 slab.

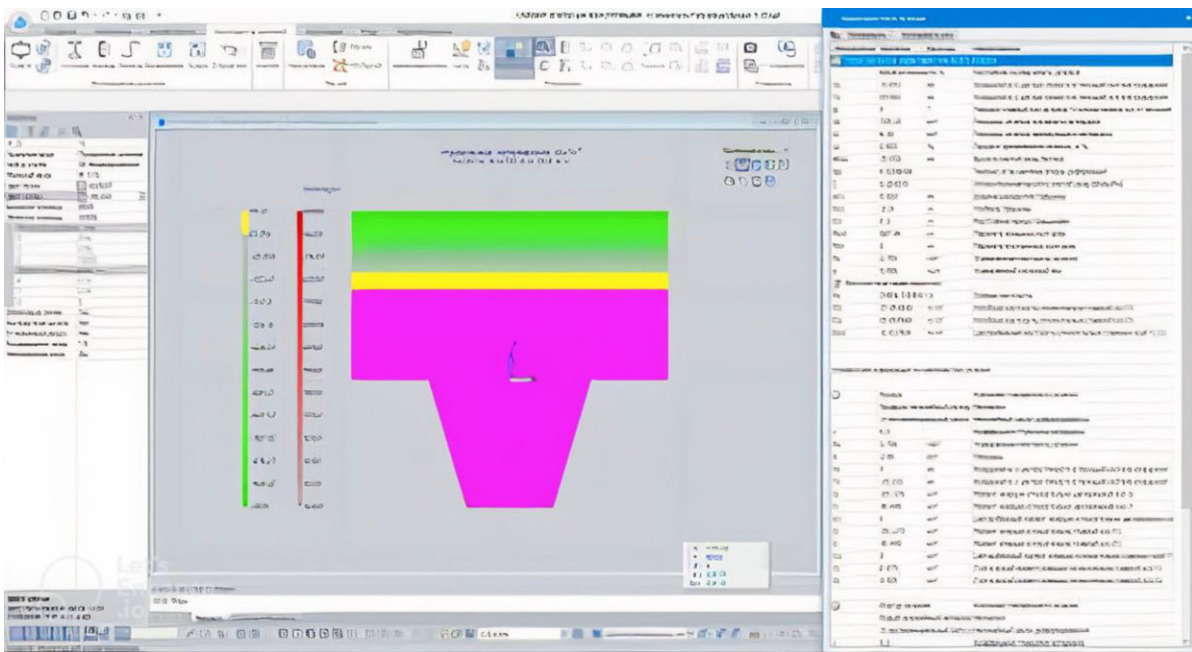


Figure 6 Geometric characteristics of the slab section.

contact—for profiled sheeting and lines formed at the intersection of cutting planes—for reinforcement. The LIRA-CAD software system was used to construct the geometric models. Profiled sheeting was the basis for the construction, where the necessary cross-sectional planes of the slab were formed.

Subsequent transformations of the basic geometric models were associated with modeling the structure of specific plates. The basic geometric models were divided into pentagons and hexagons according to the shape and arrangement of the

reinforcement by means of the LIRA-CAD software package. These divisions were performed by cutting the bodies with longitudinal planes (vertical, horizontal and inclined). The bodies were cut by curved transverse surfaces to model curvilinear reinforcement (P-2). As a result, hundreds of simple-shaped bodies were obtained, which were then meshed with finite elements (Figs 5–6). The number of bodies was 1239 (910 for the model with profiled sheeting, modeled by 2D finite elements).



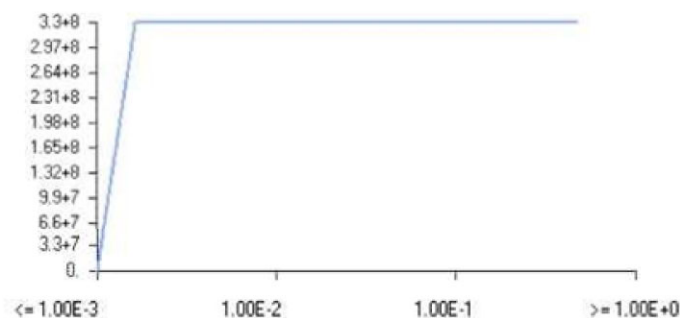


Figure 7 Curve of  $s$ - $e$  elastic-plastic model of profiled sheeting.

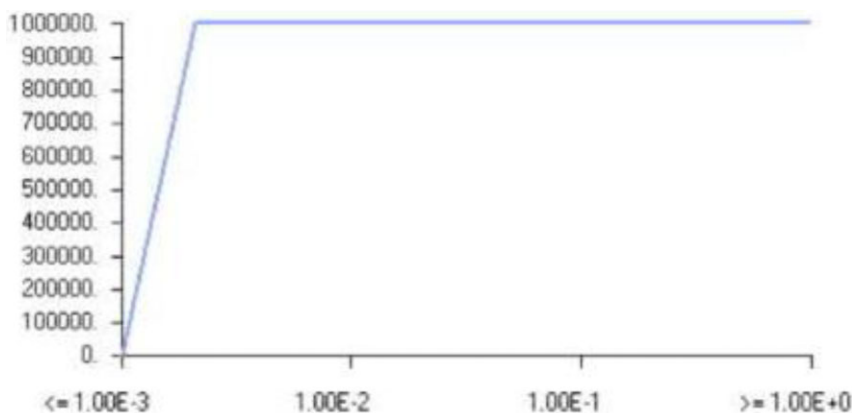


Figure 8 Curve of  $S_c$ - $E_s$  nonlinear elastic model of concrete.

### 4.3 Materials and contact modeling

The results of the experimental determination of physical and mechanical properties and the behavior of materials under load were the basis for modeling materials and contact. When modeling each material with FEM, it is necessary to set a model of its behavior (operation). The choice of one or another material operation model depends on the type of calculation used in the study of SSS in the LIRA-CAD software package and on the expected operating conditions and behavior of the material [5]. The most common models are linear-static, nonlinear-elastic, elastic-plastic (bilinear) and plastic.

Linear and static nonlinear calculations were used to study all structures in this research. According to the latter, part or all of the materials must be specified as nonlinear, indicating the model of nonlinear behavior. The type of nonlinearity selected for each of the materials is listed below. The diagrams of materials deformations calculated according to the FEM were specified in the LIRA-CAD software package in the form of functions ( $s$ - $e$ ). They were then introduced as additional characteristics in the modulus of elasticity of materials.

### 4.4 Profiled sheeting and reinforcement

Steel was a material for profiled sheeting and reinforcement. Its modulus of elasticity ( $E$ ) was equal to  $2.1 \times 10^5$  MPa, and Poisson's ratio was equal to 0.3. The displacement modulus ( $G$ ) was not specified as it is calculated automatically. The material of profiled sheeting was specified as isotropic nonlinear elastic-plastic since steel operates the same in compression and tension. Such

a model of material operation assumed a bilinear deformation curve (Fig. 7). The yield stress ( $f_y = 330$  MPa) was determined experimentally.

### 4.5 Heavy concrete

A bilinear deformation curve was constructed for steel-reinforced concrete (Fig. 8). It was based on the deformation curve of specimens (prisms). The ultimate strength and the corresponding relative deformations were the characteristic points of its construction. The experimentally determined initial modulus of elasticity and ultimate strength were equal:  $E_{ck} = 480$  MPa,  $f_{ck} = 1$  MPa. Poisson's ratio was equal to 0.1. The displacement modulus ( $G$ ) was not specified. Since heavy concrete operates differently in tension and compression, a nonlinear-elastic model of the material was used for it.

### 4.6 Contact

A piece of 0.3-mm thick mass concrete was used to model the contact. Its operation and physical and mechanical properties were the same as that of concrete up to ultimate strength. After contact deformation, these properties were not limited by anything, which corresponded to the delamination of materials and their independent deformation. The contact strength limit was also determined experimentally and was equal to 20 kPa. A nonlinear-elastic model of the material was used for the contact (Fig. 9).

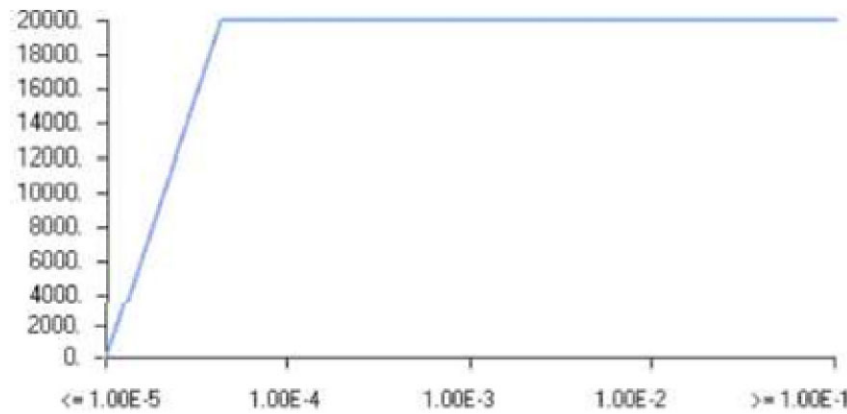


Figure 9 Curve  $S_k-E_k$  of a nonlinear-elastic model of contact.

Table 1 The type of finite elements used to model the profiled sheet and its properties.

Slab constituent	Type of FE**	Properties
Profiled sheeting	3D Solid	(1) $E = 2.1 \times 10^5$ MPa; $\nu=0.3^*$
		(2) $f_y = 330$ MPa
		(3) Elastic-plastic model
		(4) Number of nodes
2D Plate	2D Plate	(1) $E=2.1 \times 10^5$ MPa; $\nu=0.3^*$
		(2) $f_y = 330$ MPa
		(3) Elastic-plastic model
		(4) Thickness $t = 0.7$ mm
		(5) Number of nodes

\*Displacement modules were calculated automatically.

\*\*FE, finite element.

#### 4.7 Finite-elements meshing

Before meshing finite elements, their types and properties should be defined and set. In calculations presented in this research, all types of finite elements were used for modeling, including 1D, 2D, 3D and absolutely rigid finite elements (Tables 1–4).

A 1D finite element is an element that combines two adjacent nodes. It is used when the calculation conditions do not require investigation of the SSS in each exact body but determine only the highest values of stresses and strains [25]. These elements are used to model the operation of beams or rods, that is, bodies in which one size is much larger than the other two. The use of such elements corresponds to the level of design schemes for the resistance of materials when the real structure is replaced by a line or curve with characteristic sectional properties. The properties of such elements include the physical and mechanical characteristics of the material and the shape, dimensions and geometric characteristics of the cross-section.

Table 2 The type of finite elements used to model heavy concrete and its properties.

No.	Slab constituent	Type of FE**	Properties
2	Heavy concrete	3D Solid	(1) $E_{ck}=480$ MPa; $\nu=0.1^*$ (2) $f_{ck} = 1$ MPa (3) Nonlinear-elastic model (4) Number of nodes (five or six)

\*Displacement modules were calculated automatically.

\*\*FE, finite element.

Table 3 The type of finite elements used to model the contact and its properties.

No.	Slab constituent	Type of FE*	Properties
3	Contact	3D Solid	(1) $E_k=480$ MPa; $\nu=0.1^*$ (2) $f_k = 20$ kPa (3) Nonlinear-elastic model (4) Number of nodes (five or six)

\*FE, finite element.

Table 4 The type of finite elements used to model load and supports and their properties.

No.	Slab constituent	Type of FE*	Properties
5	Load, supports	Rigid	Does not change its shape but do its position in space

\*FE, finite element.

A 2D finite element is an element that combines three or four adjacent nodes. These finite elements are used to study the SSS of plates and shells, that is, bodies in which one size (thickness) is much less than the other two. These elements help determine the distribution of SSS parameters over the surface. However, the change in stresses and strains over thickness cannot be studied since they are replaced with values on the upper lower surfaces of finite elements. Examples of 2D finite element applications are pressure vessels, thin-walled structures, etc. Their main properties include the physical and mechanical characteristics of the material and the thickness of the plate or shell.

A 3D finite element is an element that most often combines four, five or six nodes. This type of finite element is effective when the SSS should be examined at each point of the body.

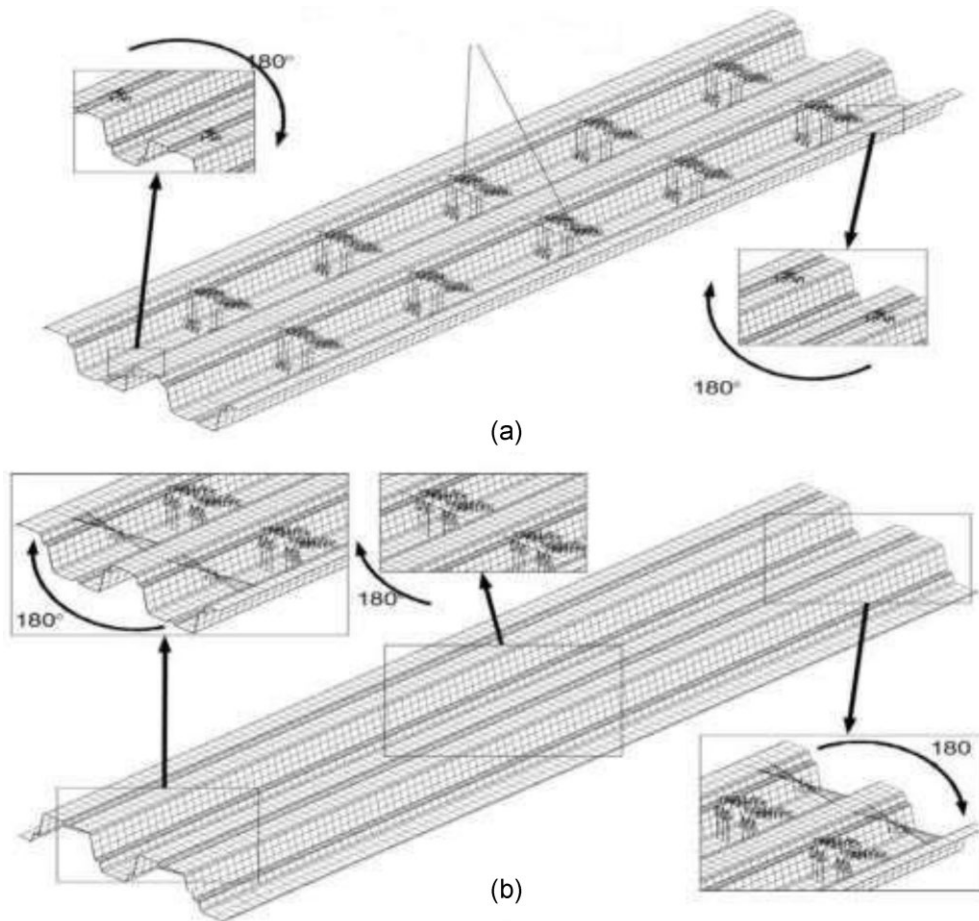


**Figure 10** Full finite element models of profiled sheeting in the positive (a) and negative (b) positions.

Three-dimensional finite elements are typically used to study massive 3D bodies, in which three dimensions are approximately the same. These elements can be in the shape of a tetrahedron, hexahedron and prism. The main properties of 3D finite elements include the physical and mechanical characteristics of the material [26].

An absolutely rigid finite element is an element that does not change its shape under the action of a load (its shape remains constant under any conditions). However, its relative position in space is changeable. An absolutely rigid finite element necessarily consists of one corresponding and one (or more) slave node. When moving the corresponding node, the entire element moves in its direction without deformation. This property can be used to model the connection between model elements but is most often used to model loads and supports.

The main condition for the correct calculation was the connectivity of meshes in the nodes that combined different materials and types of finite elements. When determining the size and configuration of meshes, they were simultaneously applied to all geometric bodies of the model.

The model consisted of a 2D finite element mesh, supports and loads. The model's simplicity made it possible to increase the number of finite elements by reducing the mesh spacing. Since the flanges of the specimens were connected by metal strips, an

absolutely rigid finite element was additionally introduced into the finite element model of the profiled sheeting; it combined the opposite flanges of the profiled sheeting model. There were five such strips in the specimens, but the finite element model contained only one. Only one strip limited deformations, while all the others lost their stability and did not affect further operation. Preliminary calculations showed that such a rigid connection impacted the calculation results for profiled sheeting since the profiled sheet itself is of a sufficiently flexible design and any measures that reduce its flexibility, and, accordingly, limit deformations, significantly affect its operation. The above also concerned the modeling of the supporting nodes of profiled sheeting. In the experiment, the flanges of profiled sheeting were additionally connected to the support, which limited the movement in the transverse direction. Accordingly, this fact was taken into account when modeling the supports (Fig. 10).

Table 5–6 presents data on the element composition of the models. The P-2 slab model was the most complex.

For all considered models, linear and nonlinear static calculations were performed. The linear static analysis ignored the nonlinear properties of materials and the geometrical nonlinearity of the structure. The calculation was based on the initial elastic modulus [27]. In this case, the delamination of materials and their destruction if the yield strength reached were

**Table 5** Element composition of models.

No.	Model	Number of finite elements by type	
		2D	3D
1	Profiled sheeting	8400	–
2	P-1	2030	7250
3	P-1	–	14 256
		2304	11 952
4	P-2	6496	40 816
5	P-3	–	12 462

**Table 6** Deflection for P1, P2 and P3 specimens.

Specimen	Load on distributing traverse, N, kN	Deflection, $f_{max}$ , cm
P1	17.5	4.58
P2	30	4.02
P3	64	1.02

impossible to study. The calculation was in accordance with Hooke's law.

#### 4.8 Calculation results and their analysis

As a matter of convenience, the calculation results were presented in the following order: profiled flooring, P-1 (grouped, similar in structure), P-2 and P-3 slabs.

#### 4.9 Profiled sheeting

Figures 11 and 12 show the von Mises stress distribution diagrams and the deformation nature of the profiled sheeting in the positive and negative positions at maximum load. As the figures show, the profiled sheeting was more rigid in the negative than in the positive position. The profiled sheeting could not move freely on supports because of more stringent ultimate conditions. According to the diagrams, the maximum stresses in the positive position arose in the support zones under the action of support reactions. In the negative position, the maximum stresses occurred within the operation zone of the maximum bending moment. In both cases, the stresses did not exceed the

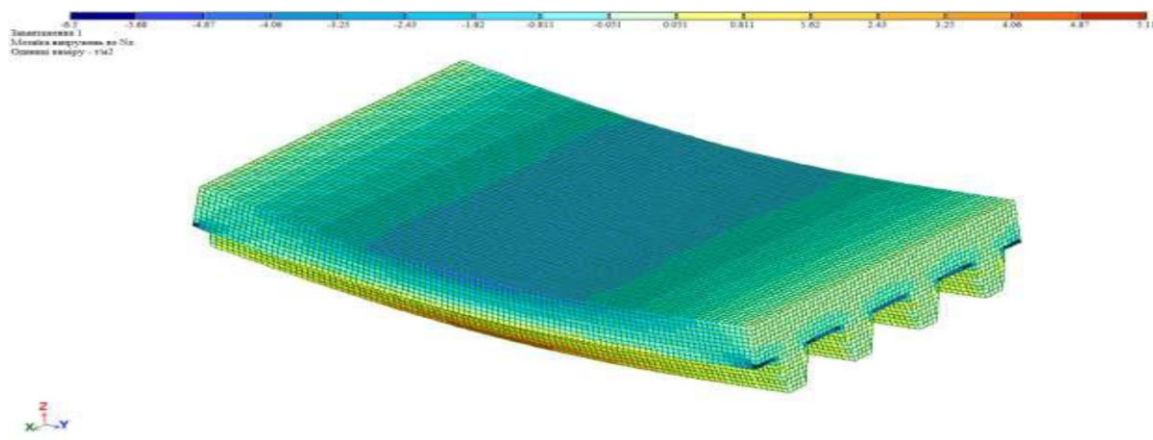
yield strength of steel (330 MPa). Weak concentrations of stress were noticeable in the middle of the span, at the locations of absolutely rigid finite elements. These stresses arose in response to the deformation limitation of the flanges of absolutely rigid finite elements.

In the positive position, strong deformations occurred at the edge points of the flanges due to their unlimited deformations. The magnitude of these deformations exceeded the deflections in the middle of the span (Table 7). Therefore, when analyzing the structure operation, attention was paid to determining the deflections at the points where deflectometers were placed.

Table 7 shows almost identical changes in deflections in the middle of the span for both positions of the profiled sheeting. This is due to the fact that the profiled sheeting is made of steel, which is a plastic isotropic material, and the ratio of the span to the height of the profiled sheeting is quite large. In this case, noticeable landslide deformations do not occur here, and the calculation results will not differ significantly from the strength of materials style calculation. However, a slight nonlinearity in the operation of the profiled sheeting is observed on the deflection graphs, caused by geometric nonlinearity, that is, a change in load conditions caused by a change in the shape of the profiled sheeting (Fig. 13) [28, 29].

As mentioned above, the P-1 slab was calculated with 2D and 3D finite element options for modeling profiled sheeting. In both cases of nonlinear calculations, the maximum experimental load value was not reached. When modeling the 2D finite element, the calculation ended at  $0.75625 F_{max}$ . When modeling the 3D finite element, the calculation ended at  $0.829687 F_{max}$ . The calculation was stopped due to the secondary buckling of the flanges of the profiled sheeting. In the case of 3D finite elements, the starting point of buckling could be fixed (Figs 14 and 15), which did not happen when using 2D finite elements. When using 2D finite elements, the starting point of buckling was determined more precisely, even before the changes in the flange geometry. The main differences in the calculations of slabs with both finite element options were as follows:

- (1) The use of 3D finite elements helps increase the load limit at which stability is lost. Changes in the

**Figure 11** The von Mises stress distribution diagram and the deformation nature of profiled sheeting in the positive position.

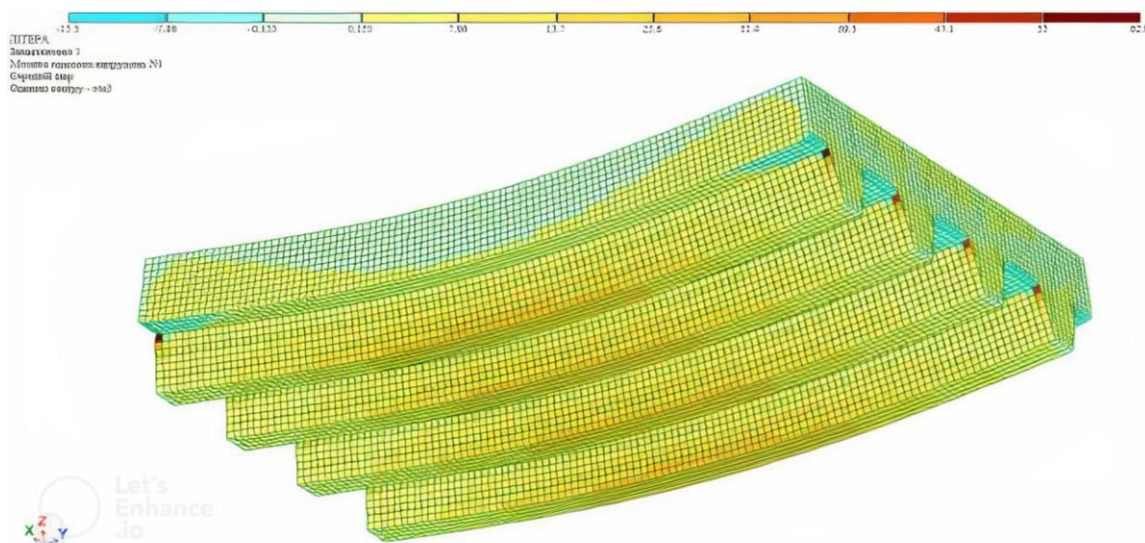


Figure 12 Stress mosaic.

Table 7 Deflections of profiled sheeting in the middle of the span at its lowest point.

Load degree	Profiled sheeting in positive position			Profiled sheeting in negative position		
	Load, N	Deflections, mm		Load, N	Deflection, mm	
		Nonlinear calculation	Linear calculation		Nonlinear calculation	Linear calculation
0	0	0	0	0	0	0
1	247	0.19	0.20	246	0.19	0.19
2	493	0.37	0.41	491	0.39	0.38
3	740	0.56	0.61	737	0.58	0.58
4	986	0.75	0.82	982	0.78	0.77
5	1233	0.95	1.02	1228	0.97	0.96
6	1479	1.14	1.23	1473	1.17	1.15
7	1726	1.34	1.43	1719	1.37	1.34
8	1972	1.54	1.64	1965	1.57	1.53
9	2219	1.74	1.84	2210	1.77	1.73
10	2465	1.94	2.05	2456	1.98	1.92
11	2712	2.15	2.25	2701	2.18	2.11
12	2958	2.36	2.46	2947	2.39	2.30
13	3205	2.57	2.66	3192	2.60	2.49
14	3451	2.78	2.87	3438	2.81	2.68
15	3698	3.00	3.07	3684	3.02	2.88
16	3944	3.22	3.28	3929	3.23	3.07
17	4191	3.44	3.48	4175	3.44	3.26
18	4437	3.67	3.68	4420	3.66	3.45

geometric shape of the body can be visualized at the buckling moment.

- (2) The use of 3D finite elements ensures better reproducibility of the calculation.
- (3) The use of 3D finite elements reduces marginally the value of deflections after delamination of materials. There were no other differences.

Figures 16 and 17 show the results of the calculation of P-1, P-2 and P-3 slabs and the dependence of the deflection on the increase in load of samples P1 (in the absence of a connection), P2 (profiled sheeting with stampings) and P3 (combination of reinforced concrete with stampings). The maximum deflections

Table 8 Dependences of the deflection on the load increase of the P1, P2 and P3 specimens.

Specimen	Load on distributing traverse, N, kN	Deflection, $f_{max}$ , cm
P1	17.5	4.58
P2	30	4.02
P3	64	1.02

determined at the middle of the span at the location of the deflectometer are shown in Table 8.

Stress concentrations were observed on all slabs along the edges of the absolutely rigid finite element of profiled sheeting

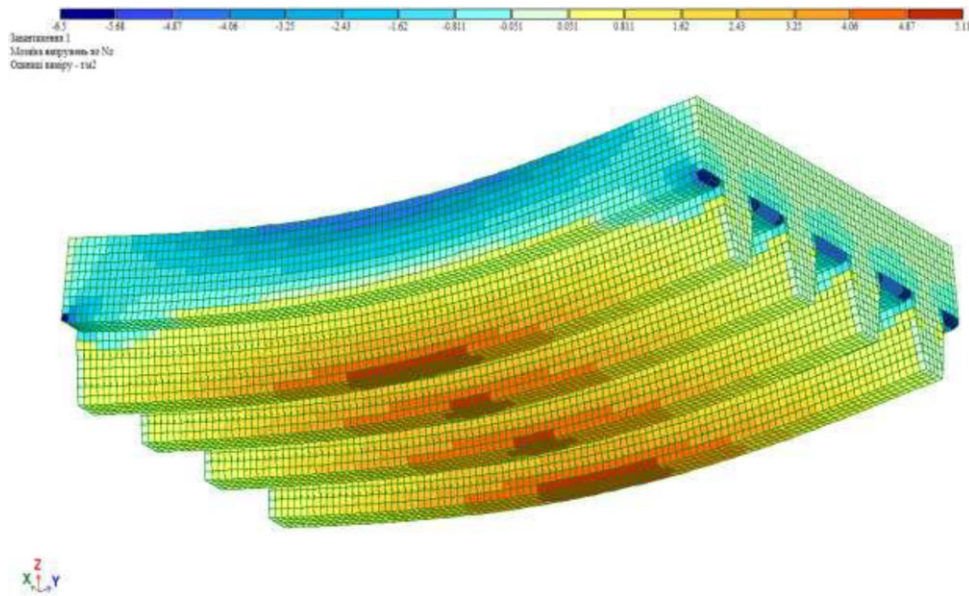


Figure 13 The von Mises stress distribution diagram and the deformation nature of the profiled sheeting in the negative position: (a) general deformations; (b) deflections in the vertical P-1, P-2 and P-3 slabs.

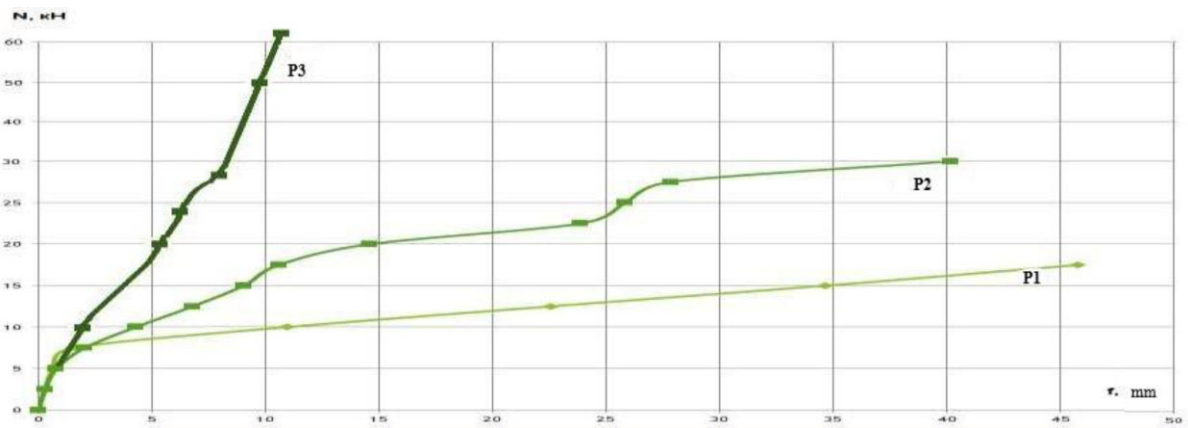


Figure 14 Dependence of the deflection on the load increase of P1, P2 and P3 specimens.

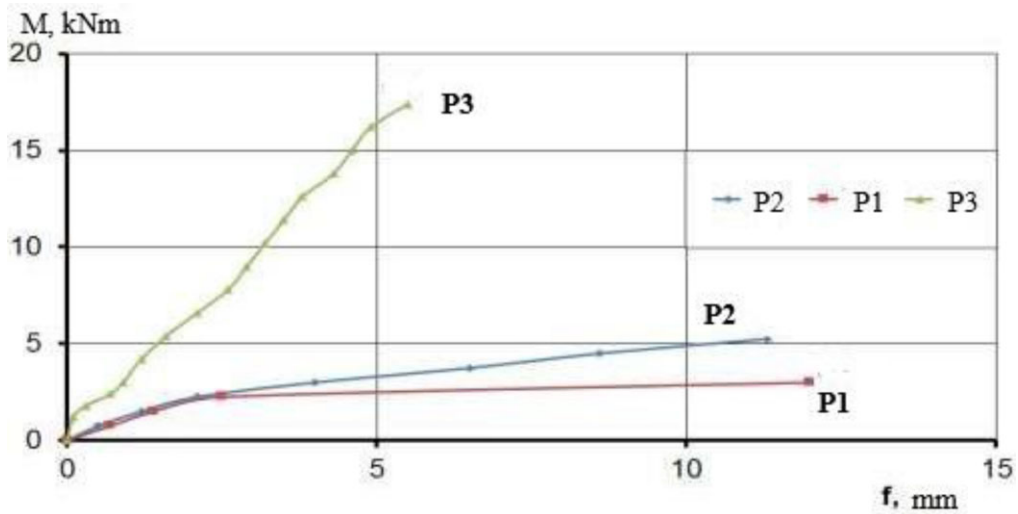


Figure 15 Bearing capacity and deflection of slab elements.

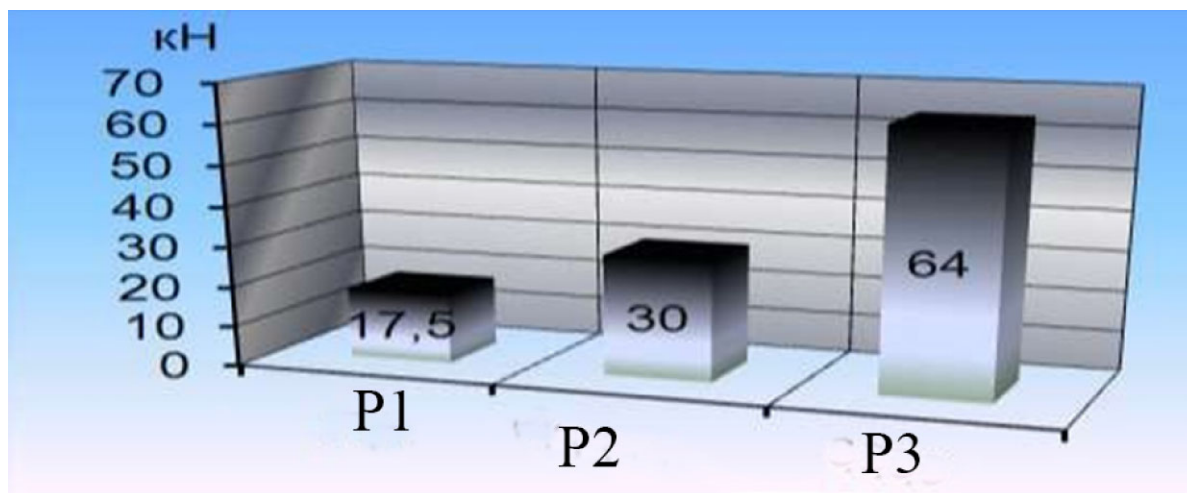


Figure 16 Bearing capacity of bending specimens.

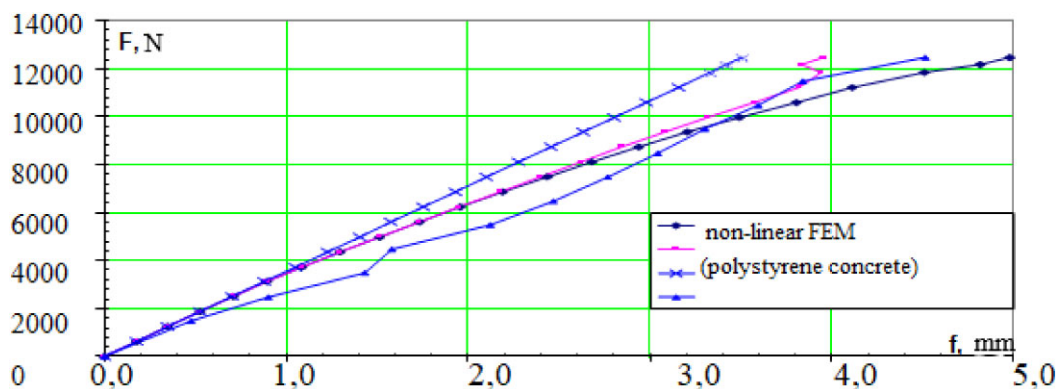


Figure 17 Comparison of deflections calculated by FEM for P-3 slab with experimental data.

Table 9 Statistical characteristics of sheet steel.

Type of steel sheet	Arithmetic mean value $\sigma$ , MPa		Sample rate, A	Root-mean-square deviation, S, MPa		Yield strength $R_{ys}$ , MPa	Tensile strength $R_{ts}$ , MPa
	$\sigma_y$	$\sigma_t$		$S_y$	$S_t$		
4 mm	252.1	374.0	3.34	2.01	5.15	247.4	356.8
12 mm	259.8	382.3	3.34	2.49	3.17	251.5	371.7

[30]. Moreover, under the “sheet” itself, there was much less tension along its edges. On the supports, the stresses reached critical values of 1 MPa under load of about 6000 N. A further load increase boosted the size of the zones with ultimate stress.

The destruction of the specimens occurred as a result of the separation of profiled sheeting from the concrete block.

## 5. EXPERIMENTAL PART OF THE STUDY

The yield strength ( $R_{ys}$ ) was taken as the main characteristic of the strength of reinforced steel, the values of which were determined with a 95% reliability, which was equivalent to the refer-

enced reinforcement strength. If the value of  $S/\sigma n > 0.1$ , the use of the results obtained according to these tests was not allowed. The results of the statistical processing of reinforced steels are given in Table 9. The results of testing the physical and mechanical properties of sheet reinforcement were as follows: steel was classified as C245 since the thickness of sheet reinforcement was 4 mm ( $\delta = 4$  mm), yield strength was 247.4 MPa ( $R_{ys} = 247.4$  MPa) and the tensile strength was 356.8 MPa ( $R_{ts} = 356.8$  MPa); steel was also classified as C245 since the thickness of sheet reinforcement was 12 mm ( $\delta = 12$  mm), yield strength was 251.5 MPa ( $R_{ys} = 251.5$  MPa) and the tensile strength was 371.7 MPa ( $R_{ts} = 371.7$  MPa).

The physical and mechanical properties of concrete were determined by testing control cubes of  $100 \times 100 \times 100$  mm and

**Table 10** Physical and mechanical properties of concrete specimens.

Composition of concrete	Strength of cube, $R_m$ , MPa	Average strength of prism, $R_{bm}$ , MPa	Tangent modulus of elasticity, $E_b$ , $10^3$ MPa	Poisson's ratio, $\nu_b$
No. 1	27.1	15.2	18.4	0.21

**Table 11** Statistical characteristics of concrete cubes-specimens.

Composition of concrete	Average strength of cubes in a batch, $R_m$ , MPa	Deviation in strength, $W_m$ , MPa	Root-mean-square deviation in a batch, $S_m$ MPa	Strength variation coefficient, $V_m$ , %	Standard compressive strength of concrete (grade of concrete), $B$ , MPa
No. 1	27.1	2.8	1.66	6.1	19.4

**Table 12** Statistical characteristics of concrete prisms-specimens.

Composition of concrete	Average strength of prisms in a batch, $R_m$ , MPa	Deviation in strength, $W_m$ , MPa	Root-mean-square deviation in a batch, $S_m$ MPa	Strength variation coefficient, $V_m$ , %	Standard compressive strength of concrete (grade of concrete), $B$ , MPa
No. 1	15.2	1.7	1	6.6	12.7

prisms of  $100 \times 100 \times 400$  mm. Table 10 shows the average strength properties of concrete. Dependence  $\sigma_b - \varepsilon_b$  for the used concrete of composition No. 1 was not directly proportional to the load. The authors determined the tangent modulus of elasticity ( $E_b$ ) and Poisson's ratio based on the obtained longitudinal and transverse deformations at a load of 30% of the breaking load. Tables 11 and 12 provide the statistical characteristics of testing concrete specimens.

The authors determined the properties of concrete specimens (cubes and prisms) through statistical analysis, that is, the average strength of cubes and prisms in a batch of specimens. These properties showed that deviations from the standard analogous indicators for each of the compositions of the concrete mixture were insignificant and did not exceed 7%. The average coefficient of concrete strength variation for all tested specimens of cubes and prisms was 6.35%.

According to the plan of experimental studies, the authors examined the operation and deformation features of the elements of slabs with profiled external reinforcement; the joint work of concrete and steel was ensured by the use of a profiled sheet with stampings. The equipment made it possible to study their work under a step static load in laboratory conditions and to obtain the characteristics of the SSS at any stage of loading (Fig. 16).

Primary fracture of the concrete block was observed with a displacement at the ends in P1 and P2 samples, in contrast to P3. It became the reason for the detachment of the profiled sheeting with subsequent deformation. However, the P3 specimen was fractured according to a slightly different scheme, which indicated a satisfactory joint operation of steel and concrete. Its profiled sheet came off instantly with the simultaneous fracture of the concrete block. The brittle fracture of concrete was due to the absence of internal reinforcement [31, 32]. Moreover, a slight increase in load did not rapidly increase deflections in the P3 specimen, which was typical for other specimens at the moment of

loss of the steel-concrete bond. Therefore, the reason for the exhaustion of the bearing capacity of the specimens is the separation of the steel profiled sheeting from the concrete.

To compare the results given above, the calculation of the P-3 slab was performed. The values of deflections in the middle of the slab span and profiled sheeting were obtained. Since profiled sheeting delaminated from heavy concrete at maximum load in the nonlinear calculation in all cases, except for the P-1 slab, the comparison averaged the deflection data for adjacent pairs of nodes (Tables 13–17).

The data in Table 17 is not indicative since they contain averages over compatible pairs of nodes in the contact, which is rather conditional. They are given to show the difference between linear and nonlinear calculation and their accuracy. Tables 17 and 18 show that the calculation overestimates the value of deflections, and the calculation using the mathematical shear model does the opposite. The error is 86% in the first case, while it reaches 36% without landslides and 28% with them in the second case. The calculations by FEM have the best reproducibility. The largest error reaches 8.4% for the P-2 slab in a nonlinear calculation. As for the linear calculation, the largest error is 34% for the P-1 and P-2 slabs.

After the approximation of the data, it was confirmed that the amount of vertical reinforcement does not affect the operation of the slabs in the linear calculation; the deflections of the P-1, P-2 and P-3 slabs turned out to be the same in the linear calculation. In a nonlinear calculation, there was an insignificant effect of the amount of reinforcement on the deformed state of slabs, which was expressed in a decrease in deflections from 4.89 to 4.07 mm. The graphs show that the FEM provided somewhat underestimated results at the initial stages of the calculation, which began to coincide during the final stages of the loads. This indicated that the slab was run in and the gap spacing was selected at the initial stages.



**Table 13** Characteristic loads for P-1 calculated by non-linear calculation model.

Span length, m	Boundary load, N/m <sup>2</sup>	Characteristic load from concrete slab, N/m <sup>2</sup>	Characteristic load from profiled sheeting, N/m <sup>2</sup>	Estimated payload, P, N/m <sup>2</sup>	Load on reinforced concrete, N, N/m <sup>2</sup>	Match condition, P N
0.50	31 168.00	1783.33	67.5	29 135.46	3250	–
0.75	13 852.44	1783.33	67.5	11 819.90	3250	–
1.00	7792.00	1783.33	67.5	5759.46	3250	yes
1.25	4986.88	1783.33	67.5	2954.34	3250	–
1.50	3463.11	1783.33	67.5	1430.57	3250	–
1.75	2544.33	1783.33	67.5	511.78	3250	–
2.00	1948.00	1783.33	67.5	–84.54	3250	–
2.25	1539.16	1783.33	67.5	–493.38	3250	–
2.50	1246.42	1783.33	67.5	–785.82	3250	–
2.75	1030.35	1783.33	67.5	–1002.19	3250	–
3.00	868.78	1783.33	67.5	–1166.76	3250	–
3.25	737.7	1783.33	67.5	–1294.84	3250	–

**Table 14** Characteristic loads for P-2 calculated by non-linear calculation model.

Span length, m	Boundary load, N/m <sup>2</sup>	Characteristic load from concrete slab, N/m <sup>2</sup>	Characteristic load from profiled sheeting, N/m <sup>2</sup>	Estimated payload, P, N/m <sup>2</sup>	Load on reinforced concrete, N, N/m <sup>2</sup>	Match condition, P N
3.50	636.08	1783.33	67.5	–1396.46	3250	–
3.75	554.10	1783.33	67.5	–1478.44	3250	–
4.00	487.00	1783.33	67.5	–1545.54	3250	–
4.25	431.39	1783.33	67.5	–1601.15	3250	–
4.50	384.79	1783.33	67.5	–1647.75	3250	–
4.75	345.35	1783.33	67.5	–1687.19	3250	–
5.00	311.68	1783.33	67.5	–1720.86	3250	–
5.25	282.70	1783.33	67.5	–1749.84	3250	–
5.50	257.59	1783.33	67.5	–1774.95	3250	–
5.75	235.67	1783.33	67.5	–1796.87	3250	–
6.00	216.44	1783.33	67.5	–1816.10	3250	–
3.50	636.08	1783.33	67.5	–1396.46	3250	–

**Table 15** Characteristic loads for P-1 calculated by linear calculation model.

Span length, m	Boundary load, N/m <sup>2</sup>	Characteristic load from concrete slab, N/m <sup>2</sup>	Characteristic load from profiled sheeting, N/m <sup>2</sup>	Estimated payload, P, N/m <sup>2</sup>	Load on reinforced concrete, N, N/m <sup>2</sup>	Match condition, P N
0.50	58 272.00	2533.33	67.5	55 416.46	3250	Yes
0.75	25 898.67	2533.33	67.5	23 041.13	3250	Yes
1.00	14 568.00	2533.33	67.5	11 710.46	3250	Yes
1.25	9323.52	2533.33	67.5	6465.98	3250	Yes
1.50	6474.67	2533.33	67.5	3617.13	3250	Yes
1.75	4756.90	2533.33	67.5	1899.36	3250	–
2.00	3642.00	2533.33	67.5	784.46	3250	–
2.25	2877.63	2533.33	67.5	20.09	3250	–
2.50	2330.88	2533.33	67.5	–526.66	3250	–
2.75	1926.35	2533.33	67.5	–931.19	3250	–
3.00	1618.067	2533.33	67.5	–1238.88	3250	–
3.25	1379.22	2533.33	67.5	–1478.32	3250	–

The most effective anchoring method was used in the P-3 slab. The method of anchoring the P-2 slab cannot be considered successful in terms of deformations and the amount of reinforcement used. As the results show (Table 18), the calculated deflections of the P-2 slab lie between the calculated deflections of the

P-3 and P-2 slabs, while the experimental ones are larger than them (Fig. 17).

Based on these findings, the anchoring method used in the P-2 slab can be recommended for use in cases where it is necessary to significantly increase the bearing capacity due to a slight decrease

**Table 16** Characteristic loads for P-2 calculated by linear calculation model.

Span length, m	Boundary load, N/m <sup>2</sup>	Characteristic load from concrete slab, N/m <sup>2</sup>	Characteristic load from profiled sheeting, N/m <sup>2</sup>	Estimated payload, P, N/m <sup>2</sup>	Load on reinforced concrete, N, N/m <sup>2</sup>	Match condition, P N
3.50	1189.22	2533.33	67.5	-1668.32	3250	-
3.75	1035.95	2533.33	67.5	-1821.60	3250	-
4.00	910.50	2533.33	67.5	-1947.04	3250	-
4.25	806.53	2533.33	67.5	-2051.01	3250	-
4.50	719.41	2533.33	67.5	-2138.13	3250	-
4.75	645.67	2533.33	67.5	-2211.87	3250	-
5.00	582.72	2533.33	67.5	-2274.82	3250	-
5.25	528.54	2533.33	67.5	-2329.00	3250	-
5.50	481.59	2533.33	67.5	-2375.95	3250	-
5.75	440.62	2533.33	67.5	-2416.92	3250	-
6.00	404.67	2533.33	67.5	-2452.88	3250	-

**Table 17** Comparison of experimental data for the P-3 slab calculated by the mathematical shear model.

Max. load, N	Experiment	Deflection, mm					
		Calculation by the recommendation		Sliding model			
		Value	Errors, %	Without sliding	Errors, %	With sliding	Errors, %
11 821	4.63	8.6	86	2.95	36	3.34	28

in the deformation properties of the slab. As for the comparison of experimental studies and the calculation of profiled sheeting, they practically coincide with each other. Nonlinear calculation of profiled sheeting should be carried out in cases where it is necessary to study in detail the operation of profiled sheeting, including its buckling. The practical part of the experiment was introduced into the construction process during the construction of the building (Fig. 18).

Thus, the theoretical part was confirmed by a practical experiment not only in laboratory conditions but also by the introduction to a real object, which achieved the highest level of development—LOD 500. Thus, after the completion of construction, the model, the point cloud and the object being constructed were put into operation. Calculations using the FEM and a mathematical shear model proved that shears affected the SSS of the structures under consideration insignificantly. Shears had the greatest impact on the strain state of slabs. Therefore, in practical calculations, the stress state can be determined using classical models and linear calculations without considering the shear.

## 6. CONCLUSION

The results obtained showed that the deformations are redistributed along and across the specimen when the load changes. In other words, if one part was the most deformed at a certain degree of loading, it would be a completely different part at the next degree. This is typical for concrete and steel, which indicates their joint operation during the entire period of the study. The distribution of relative deformations along the length of the specimens corresponded to the bending moments for the ac-

cepted loading scheme, that is, the maximum moment and deformations were noted in the middle of the span.

Studying the SSS of FEM slabs according to the developed methodology made it possible to determine the delamination of materials and identify buckling moments of flanges of profiled sheeting. It was also found that the deformations of the material, which were closer to the edge of the slab, had a value of more than 10% less than those obtained at a considerable distance. This somewhat contradicted the theoretical distribution, according to which all fibers of the section equidistant from the neutral line will have the same deformations. This was especially evident where the deformations were redistributed across the specimen. The joint operation of the structures was ensured at all stages of loading. Detachment and secondary buckling of steel elements were observed only at the destruction moment. These circumstances allow the authors to consider that these structures are reliable in operation.

The calculations made it possible to investigate the operation of profiled sheeting, the contact of materials, their delamination, the reinforcement and its effect on the SSS of heavy concrete and profiled sheeting. The most effective reinforcement was used in the P-3 slab; it can be recommended as the main type of reinforcement for steel-reinforced concrete slabs with profiled sheeting. In other cases, flexible reinforcement overstressed either heavy concrete (P-1, P-2 and P-3 slabs) or profiled sheeting (P-2). This led to longitudinal cracks and excluded reinforcement from further operation.

According to the studies performed, practical recommendations were developed for modeling and calculating steel-reinforced concrete slabs with profiled sheeting by the FEM. Furthermore, the rational choice of the type of finite element for

**Table 18** Comparison of calculation results for P-1, P-2, and P-3 slabs with experimental data.

Slab	Experiment			Nonlinear calculation					Linear calculation			
	Load at the last stage, N	Deflection, mm	Load at the last stage, N	No. node	Deflection, mm	No. Node	Deflection, mm	Middle, mm	Errors, %	Max. load, N	Deflection mm	Errors, %
P-1	11 480	4.88	11 536	19 406	5.36	3595	4.12	4.74	-	16 480	4.63	-
	12 480	5.27	12 360		5.84		4.48	5.16				
Appr.	11 821	5.01	11 821	-	5.53	-	4.25	4.89	2.4	11 821	3.32	34
	11 480	4.41	11 814	1261	4.17	2149	4.12	4.15	-	21 480	6.52	-
P-2	12 480	4.72	12 888		4.68		4.55	4.62				
	11 821	4.52	11 821	-	4.17	-	4.12	4.14	8.4	11 821	3.59	21
P-3	11 480	4.06	11 088	13 461	3.70	37 236	3.71	3.71	-	18 480	5.91	-
	12 480	4.41	12 012		4.04		4.04	4.04				
Appr.	11 821	4.18	11 821	-	3.97	-	3.97	3.97	1.0	11 821	3.0	10



**Figure 18** The use of steel-reinforced concrete floors with external reinforcement of profiled sheeting with stampings.

modeling profiled sheeting was substantiated. The SSS of steel-reinforced concrete slabs with external reinforcement by various types of profiled sheeting was compared. The calculation method allowed calculating the structures under consideration but overestimated deflection values by 86%. The same applied to the bearing capacity. Based on the calculations performed and their analysis, it follows that the FEM and a mathematical shear model can be used without considering shears to study the SSS and bearing capacity.

The experimental and theoretical results of the bearing capacity and deformability of steel-reinforced concrete slabs were compared in order to verify analytical models and determine their application. According to a nonlinear deformation model, the evaluation of the strength and stiffness of normal sections of experimental steel-reinforced concrete slabs was up to 8.1%. Recommendations were developed for the method of numerical simulation of the actual operation of steel-reinforced concrete slabs with profiled sheeting based on the FEM. Recommendations were suggested for modeling, calculating and designing steel-reinforced concrete slabs with profiled sheeting, as well as rational types of anchors to ensure the joint operation of a complex composite section.

#### ACKNOWLEDGMENTS

This research project was supported by funding from the Science and Technology Department of Ningxia, the Scientific Research Fund of North Minzu University (No. 2020KYQD40) and the China Scholarship Council under Grant (Numbers 202008100027, 202108100024).

#### REFERENCES

1. Golyshev AB, Kolchunov VI, Yakovenko IA. *Theory and Calculation of Reinforced Concrete Prefabricated Monolithic Structures Taking into Account Long-term Processes*. Kyiv: Talkom, 2013.
2. Horodetskyi OS, Genzerskyi YV. Comparative analysis of different methods of calculating seismic effects. *Bulletin of ODABA* 2018;**60**:285–292.
3. Ministry of Regions of Ukraine. *State Building Regulations. Loads and Influences. Design Standards: DBN V.1.2–2:2006. Effective from 2007-01-01*. Kyiv: Ministry of Regional Construction of Ukraine, 2006.
4. Blihar'skyi ZY. *Reconstruction and Strengthening of Buildings and Structures: Teaching Manual*. Lviv: Lviv Polytechnic University, 2008.
5. Lapenko OI. Peculiarities of operation of reinforced concrete slabs on profiled flooring. *Problems of the Development of the Urban Environment* 2017;**2**(18):89–96.
6. Bieliatyn'skyi A, Yang S, Pershakov V, Shao M, Ta M. Features of the hot recycling method used to repair asphalt concrete pavements. *Materials Science-Poland* 2022a;**40**(2):181–195.
7. Glazunov YV. Feasibility studies and scope of steel-reinforced concrete structures. *Communal Services of Cities* 2008;**80**:89–94.
8. Lapenko OI, Skrebneva DS. The method of calculating building structures with different types of corrugated board. *Problems of the Development of the Urban Environment* 2016;**2**(16):27–34.
9. Ayrumyan EL, Kamenshchikov NI, Rumyantseva IA. Features of the calculation of monolithic slabs of steel-reinforced concrete floors on profiled steel decking. *Industrial and Civil Engineering* 2015;**9**:21–26.
10. Bieliatyn'skyi A, Yang S, Pershakov V, Shao M, Ta M. Investigation of the properties and technologies of epoxy asphalt concrete preparation with the addition of fiber from fly ash of thermal power plants. *European Journal of Environmental and Civil Engineering* 2022b;**27**(5):2070–2087. <https://doi.org/10.1080/19648189.2022.2110160>
11. Bieliatyn'skyi A, Yang S, Pershakov V, Shao M, Ta M. Study of carbon nano-modifier of fly ash in cement concrete mixtures of civil engineering. *Science and Engineering of Composite Materials* 2022c;**29**(1):227–241.
12. Storozhenko LI, Lapenko OI, Nyzhnyk OV. Patent 37444 Ukraine, IPC (2006), E04B1/00. Prefabricated floor slab. statement 07/01/2008; publ. 25.11.2008, Bull. No. 22. 2006. <https://sis.nipo.gov.ua/en/search/detail/277401/>
13. Storozhenko LI, Lapenko OI, Nyzhnyk OV. Patent 43486 Ukraine, IPC (2009), E04G21/00. Reinforced concrete slab on profiled flooring. statement 17.12.2008; publ. 25.08.2009, Bull. No. 16. 2009. <https://sis.nipo.gov.ua/en/search/detail/267820/>

14. Storozhenko LI, Lapenko OI. *Reinforced Concrete Structures in Fixed Formwork*. Poltava: ASMY, 2008.
15. Karpyuk VM. *Calculation Models of the Force Resistance of Spanned Reinforced Concrete Structures in the General Case of a Stressed state*. Odesa: ODABA, 2014.
16. Abdal S, Mansour W, Agwa I, Nasr M, Abadel A, Onuralp Özkılıç Y, Akeed MH. Application of ultra-high-performance concrete in bridge engineering: current status, limitations, challenges, and future prospects. *Buildings* 2023;**13**(1):185. <https://doi.org/10.3390/buildings13010185>
17. Góra J, Piasta W. Impact of mechanical resistance of aggregate on properties of concrete. *Case Studies in Construction Materials* 2020;**13**:e00438. <https://doi.org/10.1016/j.cscm.2020.e00438>
18. Ho LS, Huynh T-P. Long-term mechanical properties and durability of high-strength concrete containing high-volume local fly ash as a partial cement substitution. *Results in Engineering* 2023;**18**:101113. <https://doi.org/10.1016/j.rineng.2023.101113>
19. Hong S-H, Choi J-S, Yuan T-F, Yoon Y-S. A review on concrete creep characteristics and its evaluation on high-strength lightweight concrete. *Journal of Materials Research and Technology* 2023;**22**:230–251. <https://doi.org/10.1016/j.jmrt.2022.11.125>
20. Sánchez-Olivares G, Tomás A. Optimization of reinforced concrete sections under compression and biaxial bending by using a parallel firefly algorithm. *Applied Sciences* 2021;**11**(5):2076. <https://doi.org/10.3390/app11052076>
21. Yu Z, Shen L, Tang R, Huang Q. An experimental study and failure mechanism analysis on dynamic behaviors of plain concrete under biaxial compression-compression. *Case Studies in Construction Materials* 2022;**17**:e01200. <https://doi.org/10.1016/j.cscm.2022.e01200>
22. Wang C-H, Zhao J, Li J, Liu K, Braithwaite CH, Zhang Q-B. Dynamic mechanical properties and fracturing behaviour of concrete under biaxial compression. *Construction and Building Materials* 2022;**301**:124085. <https://doi.org/10.1016/j.conbuildmat.2021.124085>
23. Wang S, Xu L, Li B, Liu S, Chi Y. Mechanical behavior and stress-strain model of steel-polypropylene hybrid fiber reinforced ultra-high performance concrete under triaxial compression. *Construction and Building Materials* 2024;**450**:138595. <https://doi.org/10.1016/j.conbuildmat.2024.138595>
24. Ministry of Regions of Ukraine. *State Building Regulations. Steel Structures. Design Norms: DBN V.2.6.-198:2014*. Effective from 2015-01-01. Kyiv: Ministry of Regional Construction of Ukraine, 2014.
25. Lapenko OI. The problem of ensuring the compatible operation of concrete and steel in steel-reinforced concrete structures. *Urban Planning and Territorial Planning* 2013;**48**:255–260.
26. Zamaliev FS. Numerical experiments in the study of the spatial work of steel-reinforced concrete floors. *News of KGASU* 2012;**4**(22): 102–107.
27. Fraquiacomo M, Amadio C, Macorini L. Finite-element model for collapse and long-term analysis of steel-concrete composite beams. *Journal of Structural Engineering* 2004;**3**(3):489–497.
28. Balomenos GP, Genikomsou AS, Polak MA, Pandey MD. Efficient method for probabilistic finite element analysis with application to reinforced concrete slabs. *Engineering Structures* 2015;**103**:85–101.
29. Fraile-Garcia E, Ferreiro-Cabello J, Martinez-Camara E, Jimenez-Macias E. Frail Optimization based on life cycle analysis for reinforced concrete structures with one-way slabs. *Engineering Structures* 2016;**109**:126–138.
30. Mursi M, Uy B. Strength of concrete-filled steel box columns incorporating interaction buckling. *Journal of Structural Engineering* 2003;**5**(5):626–639.
31. Lapenko OI. Problems of reinforcing concrete with invisible formwork. *Construction, Materials Science, Mechanical Engineering* 2009;**50**:279–284.
32. Yang S, Bieliatynskyi A, Pershakov V, Shao M, Ta M. Asphalt concrete based on a polymer-bitumen binder nanomodified with carbon nanotubes for road and airfield construction. *Journal of Polymer Engineering* 2022;**42**(5):458–466.